

Rutherford scattering diagnostic for the Madison symmetric torus reversed-field pinch

J. C. Reardon, G. Fiksel, and C. B. Forest

Department of Physics, University of Wisconsin—Madison, Madison, Wisconsin 53706

A. F. Abdrashitov, V. I. Davydenko, A. A. Ivanov, S. A. Korepanov, S. V. Murachtin, and G. I. Shulzhenko

Budker Institute of Nuclear Physics, Novosibirsk 630090, Russia

(Presented on 19 June 2000)

The technique of Rutherford scattering (RS) has been used (for the first time on a reversed-field pinch) to measure the bulk majority ion temperature on the Madison symmetric torus (MST). RS has been in routine operation on MST since December 1999. The neutral beam source and electrostatic energy analyzers which comprise the RS diagnostic were built by the Budker Institute of Nuclear Physics (Novosibirsk, Russia). The source is described in another paper (Abdrashitov *et al.*, these proceedings) and the analyzers are described. A data analysis routine has been developed which yields accurate fits to the data, and estimates of errors in the fit parameters. Typical results are shown. © 2001 American Institute of Physics. [DOI: 10.1063/1.1321737]

I. INTRODUCTION

The use of a neutral beam to determine the bulk majority ion temperature of a gas or plasma, by measuring the small-angle scattering of the beam atoms, was first proposed in 1972.¹ This technique requires the neutral beam be approximately mono-energetic, with energy much greater than the temperature of the plasma. Some of the beam atoms will undergo small-angle Coulomb scattering off of plasma ions without being ionized (hence the name, *Rutherford scattering*), and will retain information about the ion velocity distribution f_i . In particular, upon the assumption that f_i is Maxwellian, the ion temperature T_i can be found from the width of the energy spectrum of the scattered atoms. In the simplest case, a mono-energetic beam (of energy E_0) with zero angular spread, the energy spectrum of atoms scattered by angle $\theta \ll 1$ is approximately Gaussian, with a variance Δ and a centroid E_c given by²

$$\Delta = \sqrt{2\mu E_0 T_i \theta^2}, \quad E_c = E_0(1 - \mu \theta^2), \quad (1)$$

where $\mu = m_b/m_i$. (There is an additional shift in E_c caused by nonzero bulk ion flow velocity, which will be neglected here.) Typically, θ is chosen to be about 10° as a compromise between improved accuracy and decreasing signal (due to the well-known $1/\sin^4 \theta$ dependence of the Coulomb scattering cross-section). A complication arises for a real beam with nonzero energy spread and angular divergence, since in this case a detector at a fixed location observes atoms which have undergone scattering by a range of angles θ , and the θ dependence in the Coulomb cross-section results in a non-Gaussian spectrum. In addition, a real analyzer with a finite acceptance angle will record scatterings which have occurred over a finite volume. RS has seen limited use by the fusion community, on the tokamaks T-4,³ JT-60,⁴ and TEXTOR,⁵ and on the mirror GDT.⁶

II. APPARATUS

The RS diagnostic consists of a 20 KV DINA-5F neutral beam source,⁷ which produces a 4 A equivalent-current beam of helium atoms for a duration of 3 ms, and two 12-channel electrostatic energy analyzers, all of which were designed and constructed at the Budker Institute of Nuclear Physics in Novosibirsk, Russia (and delivered to the University of Wisconsin on time and within budget). A cross-section of one of the analyzers is shown in Fig. 1. Scattered atoms enter from below after being collimated by passing through two slits, of widths 6 and 12 mm, separated by 33 cm (seven baffles are inserted between these two slits, in order to reject atoms reflected by the sides of the tube). The atoms then pass through a stripping cell filled with hydrogen gas, and some are ionized. A few of the ions then pass through a 1 mm slit in the lower plate of the 45° electrostatic analyzer, and encounter an electrostatic field perpendicular to the plates. The range of the ion (measured along the lower plate) is proportional to the ion's incident velocity. The voltages of the analyzer plates are provided by tapping into the beam voltage source. This is done in order to compensate for any droop in the beam voltage (which is observed to be less than 10%). Ions in a selected energy range are detected by a 12-anode multi-channel plate (MCP) with a current amplification factor of 10³; the energy range for this set of experiments was 0.75 < E/E_0 < 1.1. The current from each channel is sent to a solid-state current-to-voltage amplifier with a transimpedance of 10⁶ V/A, so that an incident ion current of 20 pA produces an output voltage of 0.02 V, typical of the maximum signal from a hydrogen plasma. Voltages from all 24 channels are digitized at 1 MHz, while the beam voltage is digitized at 100 kHz; the digitizers are controlled via CAMAC and data is stored on a VAX.

The source and the analyzers are installed on MST⁸ as shown in Fig. 2. The axes of the two analyzers can be tilted or translated independently. For this set of experiments, both

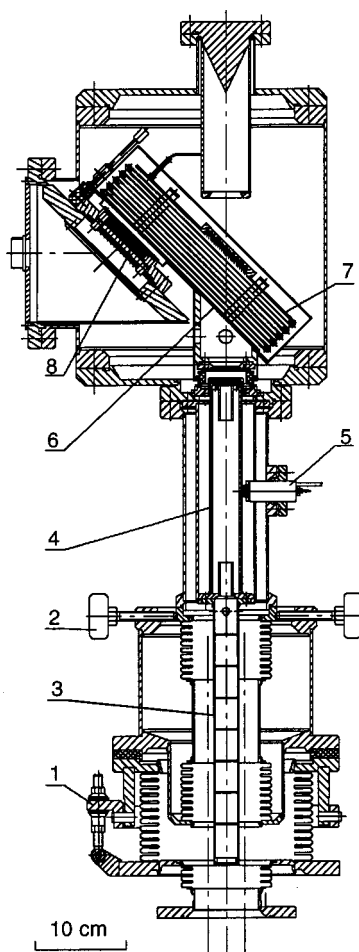
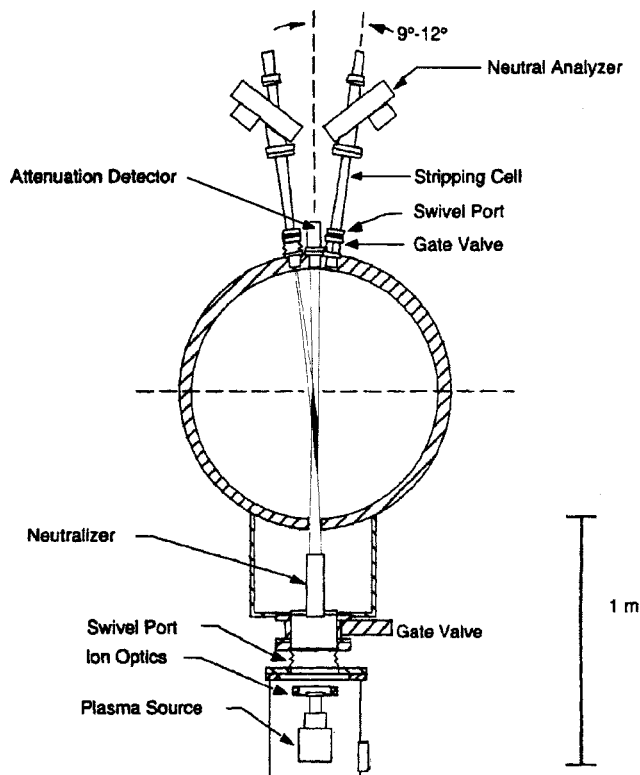


FIG. 1. Diagram of Rutherford scattering neutral particle analyzer, showing (1) tilt adjust; (2) translate adjust; (3) collimation tube; (4) stripping cell; (5) hydrogen puff valve; (6) 45° electrostatic energy analyzer, bottom plate; (7) 45° electrostatic energy analyzer, top plate; and (8) MCP.

analyzer axes were tilted by 10.2° to the vertical, and each analyzer axis was translated so that the analyzer sight-line intersected the beam axis approximately 15 cm below MST midplane. The scattering volume, formed by the intersection of the beam and the analyzer sight-lines, has a radial extent of about 30 cm, and is shown as the dark region near the center of MST in Fig. 2. All data presented here are from one of the analyzers. Comparison of spectra from the two analyzers will allow measurement of the poloidal ion flow velocity, which would cause opposite energy shifts in the spectra of the two analyzers. This shift is expected to be small and was not obvious in the present data set.

III. DATA ANALYSIS

Typical raw data is shown in Fig. 3. The voltage from channel 8 is shown as a function of time in the lower plot, and the energy spectrum (averaged between the times of the two vertical lines) is shown in the upper plot. The beam energy is represented by the vertical line in the upper plot. For each channel, a baseline is calculated both before and after the beam turns on, and a linear interpolation is then computed and subtracted. Some of the fluctuations that can be seen in the lower plot are due to fluctuations in the beam density or the plasma density, and are coherent across all of



Rutherford scattering diagnostic on MST.

FIG. 2. Rutherford scattering source and analyzers, as installed on MST. The scattering volume is the black region near the center of MST.

the channels. Before analysis, the signal from channel 12 (the highest energy channel) is subtracted from each channel in order to remove these coherent fluctuations. After the baseline is subtracted, the data is divided into nine 300 μ s segments (rejecting data at the start and end of the beam) and averaged. The averaged data thus consists of nine 12-point spectra for each analyzer for each plasma discharge.

One signal of non-RS-origin was observed. This signal

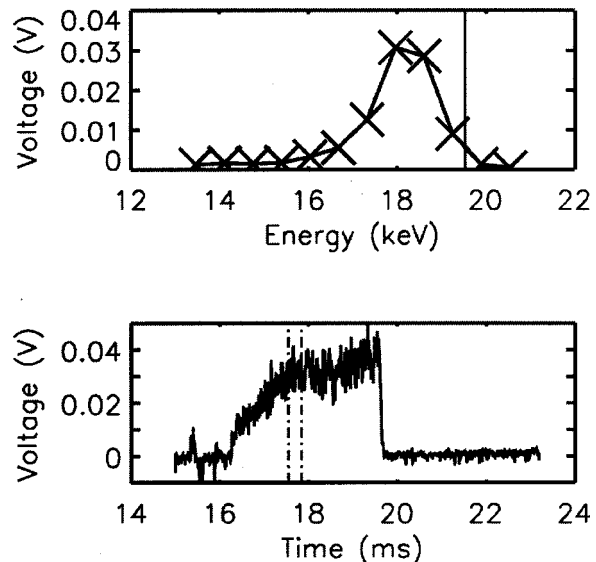


FIG. 3. Typical raw data, and spectrum, from 200 kA deuterium plasma.

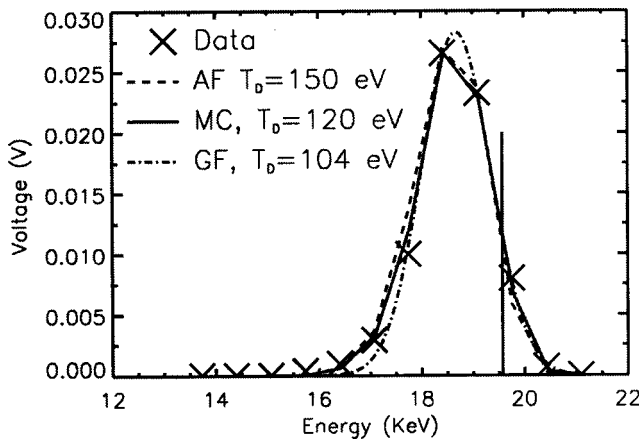


FIG. 4. Comparison of analytic fit [“AF,” Eq. (4), with $T_D = 150$ eV, dashed line], Monte Carlo simulation [“MC,” based on Eq. (3), with $T_D = 120$ eV, solid line], and Gaussian fit [“GF,” Eq. (1), with $T_D = 104$ eV, dot-dash line] to data from a 200 kA deuterium plasma.

took the form of a peak centered between channels 2 and 3, and became large when the analyzer was pointed to look directly at the port from which the beam emerged; it was attributed to inelastic scattering of the beam atoms from the

sides of the port. Its spectral shape was characterized by firing the beam into vacuum, so that the RS signal disappeared. The non-RS signal was then subtracted from the data on the assumption that it was entirely responsible for the signal on channel 3 (for which the RS signal is expected to be very small). The spectrum shown in Fig. 3 is before subtraction; the spectrum shown in Fig. 4 is after subtraction.

Great care was taken in determining the best algorithm to fit the data. Previous theoretical work^{9,10} leads to the following expression for the energy distribution $f(E)$ of scattered atoms in the case of an ideal beam:

$$f(E) = C \left[\frac{Z_p Z_b e^2}{4 \pi \epsilon_0} \right]^2 \frac{1}{E_0^2} \sqrt{\frac{\pi E}{\mu T_i}} \frac{1}{\sin^4 \theta} \times \exp \left\{ \frac{-(E - E_0(1 - \mu \sin^2 \theta))^2}{4 \mu E_0 T_i} \right\}, \quad (2)$$

where the initial factor C includes detector efficiency, beam attenuation by plasma, and probability of RS as compared with charge exchange, all of which are assumed to be independent of the final energy of the atom. In order to account for the finite beam energy spread and finite scattering volume, we write

$$f(E) = f_0 \int \int dE_0 d\theta e^{-(E_0 - \mathcal{E})^2/2\Delta E_0^2} e^{-(E - E_0(1 - \mu \sin^2 \theta))^2/4\mu E_0 T_i \theta^2} e^{-(\theta_c - \theta)^2/2\Delta \theta^2} \frac{\sqrt{E}}{\sin^4 \theta}, \quad (3)$$

where \mathcal{E} , the beam energy centroid, is taken to be the digitized beam voltage. The three parameters are θ_c , the effective average scattering angle; ΔE_0 , the beam energy spread, and $\Delta \theta$, which includes the effects of the beam spatial width, the beam angular divergence, and the acceptance angle of the analyzer. These three parameters are determined from fitting the data from scattering on room-temperature hydrogen (or deuterium) gas, for which the second exponential factor may be approximated as a Dirac δ -function. For plasma, the broadening of $f(E)$ caused by T_i cannot be neglected (indeed, it is the goal of the measurement) and only the integral over dE_0 is analytic. We approximate $\theta \sim \theta_c$ in the $1/\sin^4 \theta$ term, and making use of the small angle approximation find that $f(E)$ can be written

$$f(E) = f_0 \sqrt{E} \frac{\sqrt{\pi} \Delta_2}{\sqrt{\Delta_1^2 \Delta_2^2 + \Delta_2^2 \Delta_3^2 + \Delta_3^2 \Delta_1^2}} \times \exp \left\{ \frac{-(\Delta_1^2 (E_2 - E_3)^2 + \Delta_2^2 (E_3 - E_1)^2 + \Delta_3^2 (E_1 - E_2)^2)}{\Delta_1^2 \Delta_2^2 + \Delta_2^2 \Delta_3^2 + \Delta_3^2 \Delta_1^2} \right\}, \quad (4)$$

where

$$E_1 = -\theta_c, \quad \Delta_1^2 = \frac{\Delta \theta^2 - 4 \theta_c \Delta \theta}{4 \ln(1 - \Delta \theta / \theta_c)},$$

$$E_2 = \sqrt{\frac{\mathcal{E} - E}{\mathcal{E} \mu}},$$

$$\Delta_2^2 = \frac{4 \theta_c^2 T_i}{\mathcal{E} \mu} \frac{1 + (\Delta E_0^2 / 2\mu \mathcal{E} T_i \theta_c^2)(1 - \mu \sin^2 \theta_c)^2}{(\theta_c - \sqrt{(\mathcal{E} - E)/\mathcal{E} \mu})^2},$$

$$E_3 = \theta_c, \quad \Delta_3^2 = 2 \Delta \theta^2.$$

Using this equation, there are two free parameters to be fit to the data, f_0 and T_i .

Typical fits (corresponding to the data shown in Fig. 3) are shown in Fig. 4. The analytic fit to Eq. (4) (AF, dashed line) gives $T_i = 150$ eV, while a Monte Carlo simulation based on Eq. (3) (MC, solid line) gives $T_i = 120$ eV, a slightly smaller temperature corresponding to a slightly narrower peak width. Both fits reproduce the “tail” on the low-energy side of the peak (channels 5 and 6), but the Monte Carlo fit typically has slightly smaller χ^2 . Thus the result of the Monte Carlo fit is used as the measured value of T_i . The Gaussian fit to Eq. (1) (GF, dot-dash line) does not reproduce the low-energy tail and gives a substantially higher χ^2 , and lower T_i , than the other methods. However, the time variations of temperatures from the three fits are similar, allowing the much faster Gaussian fit to be used to provide quick overviews of the data.

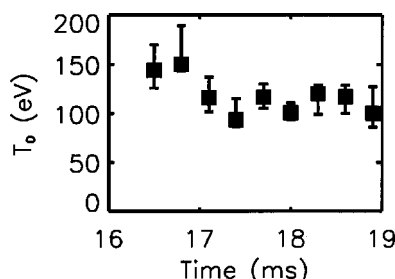


FIG. 5. The T_i measurements during a 200 kA discharge in deuterium. Error bars are estimated from the variance σ^2 between the measured spectrum and the Monte Carlo fit.

IV. ERROR ANALYSIS

It is difficult to calculate rigorously the error in T_i from the fit, because the errors in the 12 detector signals are not known. We estimate the error in the fit T_i by a statistical method based on the variance σ^2 between the measured spectrum and the Monte Carlo fit. An ensemble of simulated spectra is created, each of which has a variance of σ^2 relative to the fit. The deviations of each point in a simulated spectrum from the corresponding point in the fit are assigned at random, subject to the constraint on the total variance. These simulated data sets are then themselves fit, resulting in a range of simulated T_i measurements. The error in fit T_i corresponds to the median 50% of the simulated T_i measurements. Typical data from a 200 kA deuterium discharge are shown in Fig. 5. The error in the fit T_i due to noise in the detector signals (indicated by the error bars) is smaller than the variation in T_i during the discharge.

V. SUMMARY AND FUTURE WORK

Measurements have been made using the RS diagnostic on a wide range of MST plasmas. The diagnostic has operated reliably in all conditions. A data analysis routine has been developed which rejects non-RS signals and provides estimates of T_i with associated error bars. Measurements of T_i during scans of plasma density and plasma current in both hydrogen and deuterium discharges have been made and are being compared to measurements from other diagnostics. Work has begun attempting to understand these measurements using simple transport models. Comparison of the spectra measured by the two analyzers will soon be attempted, resulting in an estimate of the poloidal ion flow velocity. Modification of the analyzers to improve signal without decreasing T_i resolution is under discussion.

- ¹V. G. Abramov, V. V. Afrosimov, I. P. Gladkovskii, A. I. Kislyakov, and V. I. Perel', Sov. Phys. Tech. Phys. **16**, 1520 (1972).
- ²E. L. Berezovskii, A. I. Kislyakov, S. Y. Petrov, and G. V. Roslyakov, Sov. J. Plasma Phys. **6**, 760 (1980).
- ³E. V. Aleksandrov *et al.*, JETP Lett. **29**, 1 (1979).
- ⁴K. Tobita *et al.*, Nucl. Fusion **28**, 1719 (1988).
- ⁵A. A. E. van Blokland *et al.*, Rev. Sci. Instrum. **63**, 3359 (1992).
- ⁶A. V. Anikeev *et al.*, Phys. Plasmas **4**, 347 (1997).
- ⁷A. F. Abdrashitov *et al.*, Rev. Sci. Instrum. (these proceedings).
- ⁸R. N. Dexter, D. W. Kerst, T. W. Lovell, S. C. Prager, and J. C. Sprott, Fusion Technol. **19**, 131 (1991).
- ⁹R. K. B. Helbing, J. Chem. Phys. **48**, 472 (1968).
- ¹⁰K. H. Burrell, A. F. Lietzke, and M. J. Schaffer, IEEE Trans. Plasma Sci. **PS-6**, 107 (1978).